

May 2013

Direct detection experiments explained with mirror dark matter

R. Foot¹

*ARC Centre of Excellence for Particle Physics at the Terascale,
School of Physics, University of Melbourne,
Victoria 3010 Australia*

Recently, the CDMS/Si experiment has observed a low energy excess of events in their dark matter search. In light of this new result we update the mirror dark matter explanation of the direct detection experiments. We find that the DAMA, CoGeNT, CRESST-II and CDMS/Si data can be simultaneously explained by halo $\sim Fe'$ interactions provided that $v_{rot} \approx 200$ km/s. Other parameter space is also possible. Forthcoming experiments, including CDMSlite, CDEX, COUPP, LUX, C-4,... should be able to further scrutinize mirror dark matter and closely related hidden sector models in the near future.

¹E-mail address: rfoot@unimelb.edu.au

The experimental effort to directly detect dark matter has been progressing extremely well over the last decade. Impressive positive results have been reported by DAMA [1, 2], CoGeNT[3, 4], CRESST-II[5] and now CDMS/Si[6]. Previous work[7, 8] (see also ref.[9] for earlier studies) has shown that the positive results from the DAMA, CoGeNT and CRESST-II experiments can be self consistently explained within the framework of mirror dark matter (for a review see e.g.[10] and references there-in for a more complete bibliography). More generic hidden sector dark matter models are also possible[11]. The purpose of this note is to update the mirror dark matter explanation in light of the new results from the CDMS/Si experiment.

Recall, mirror dark matter features a hidden sector which is isomorphic to the ordinary sector. That is, interactions are described by the Lagrangian[12]:

$$\mathcal{L} = \mathcal{L}_{SM}(e, \mu, u, d, A_\mu, \dots) + \mathcal{L}_{SM}(e', \mu', u', d', A'_\mu, \dots) + \mathcal{L}_{mix}. \quad (1)$$

The theory contains an exact and unbroken parity symmetry: $x \rightarrow -x$ provided that left and right chiral fields are interchanged in the mirror sector. The \mathcal{L}_{mix} part denotes terms coupling the two sectors together. Chief among these is kinetic mixing of the $U(1)_Y$ and $U(1)'_Y$ gauge bosons which is a gauge invariant and renormalizable interaction[13]. This $U(1)$ kinetic mixing implies also photon-mirror photon kinetic mixing:

$$\mathcal{L}_{mix} = \frac{\epsilon}{2} F^{\mu\nu} F'_{\mu\nu} \quad (2)$$

where $F_{\mu\nu}$ and $F'_{\mu\nu}$ are the field strength tensors for the photon and mirror photon respectively. One effect of the kinetic mixing interaction is to give the mirror electron and mirror proton a tiny ordinary electric charge, ϵe [14]. This means that a mirror nucleus, A' , with atomic number Z' and velocity v can Rutherford scatter off an ordinary nucleus, A , with atomic number Z . The cross-section for this process is given by

$$\frac{d\sigma}{dE_R} = \frac{2\pi\epsilon^2 Z^2 Z'^2 \alpha^2 F_A^2 F_{A'}^2}{m_A E_R^2 v^2} \quad (3)$$

where F_A [$F_{A'}$] is the form factor which takes into account the finite size of the nucleus [mirror nucleus]². The Helm form factor[15, 16] is used in our numerical work.

The astrophysics and cosmology of kinetically mixed mirror dark matter has been discussed in a number of articles e.g. [17, 18, 19, 20, 21, 22]. A consistent picture appears to be emerging: Mirror dark matter can be the inferred dark matter in the Universe provided kinetic mixing exists with strength $\epsilon \sim 10^{-9}$. In this scenario, dark matter halos in spiral galaxies are presumed to be composed of mirror particles in a pressure supported multi-component plasma containing e' , H' , He' , O' , Fe' , ...[17]. Such a plasma dissipates energy due to thermal bremsstrahlung and other processes and this energy must be replaced. Studies have shown[17, 22] that ordinary supernovae can supply this energy if photon-mirror photon kinetic mixing has strength $\epsilon \sim 10^{-9}$ and the halo contains a significant mirror metal component ($\gtrsim 1\%$ by mass).

The mirror metal component can be probed in current direct detection experiments. The rate depends on the dark matter distribution which is assumed to be Maxwellian

²Unless otherwise indicated, natural units with $\hbar = c = 1$ are used.

with a temperature, T . This temperature can be roughly estimated from the hydrostatic equilibrium condition[17]:

$$T \simeq \frac{1}{2} \bar{m} v_{rot}^2 \quad (4)$$

where $v_{rot} \sim 240$ km/s is the galactic rotational velocity and $\bar{m} = \sum n_{A'} m_{A'}/\sum n_{A'}$ is the mean mass of the mirror particles in the halo³. In our numerical work we set $\bar{m} \approx 1.1$ GeV which is suggested by mirror BBN computations for $\epsilon \sim 10^{-9}$ [20]. The halo distribution of a mirror nuclei, A' , is:

$$f_{A'}(\mathbf{v}, \mathbf{v}_E) = \exp(-E/T) = \exp(-\frac{1}{2} m_{A'} \mathbf{u}^2/T) = \exp(-\mathbf{u}^2/v_0^2) \quad (5)$$

where $\mathbf{u} = \mathbf{v} + \mathbf{v}_E$. Here \mathbf{v} is the velocity of the halo particles in the Earth's reference frame and \mathbf{v}_E is the velocity of the Earth around the galactic center⁴ [$\langle v_E \rangle = v_{rot} + 12$ km/s]. Clearly

$$v_0[A'] = \sqrt{\frac{2T}{m_{A'}}} \simeq v_{rot} \sqrt{\frac{\bar{m}}{m_{A'}}}. \quad (6)$$

Evidently, the quantity $v_0[A']$ which characterises the velocity dispersion of the particle A' depends on the mass of the particle. This result, along with the recoil energy dependence of the Rutherford scattering cross-section [$d\sigma/dE_R \propto 1/E_R^2$] are important distinguishing features of mirror dark matter (and more generic hidden sector models with unbroken $U(1)'$ gauge interactions).

The rate for A' scattering on a target nuclei, A , is

$$\frac{dR}{dE_R} = N_T n_{A'} \int_{|\mathbf{v}| > v_{min}}^\infty \frac{d\sigma}{dE_R} \frac{f_{A'}(\mathbf{v}, \mathbf{v}_E)}{v_0^3 \pi^{3/2}} |\mathbf{v}| d^3 \mathbf{v} \quad (7)$$

where the integration limit is $v_{min} = \sqrt{(m_A + m_{A'})^2 E_R / 2m_A m_{A'}}$. In Eq.(7), N_T is the number of target nuclei and $n_{A'} = \rho_{dm} \xi_{A'}/m_{A'}$ is the number density of the halo A' particles. [$\rho_{dm} = 0.3$ GeV/cm³ and $\xi_{A'}$ is the halo mass fraction of species A']. The integral, Eq.(7), can be expressed in terms of error functions and numerically solved.

Detector resolution effects can be included by convolving the rate with the appropriate Gaussian distribution. The relevant rates for the DAMA, CoGeNT, CRESST-II and CDMS/Si experiments can then be computed and compared with the data. Note that the H' , He' halo components are too light to give significant signal contributions due to exponential kinematic suppression. For these experiments only heavier ‘metal’ components can give an observable signal above the detector energy thresholds. For simplicity we assume that the rate in each experiment is dominated by the interactions of a single such metal component, A' . Naturally this is only an approximation, however it

³This rough estimate assumed an isothermal halo. In reality, the temperature is not expected to be constant, but increases towards the galactic center. However, numerical work indicates[22] that the temperature at the Sun's location is roughly consistent (i.e. within around 20%) with the estimate Eq.(4).

⁴We have neglected here the possibility of any bulk halo rotation. In the presence of bulk halo motion, \mathbf{v}_E is the velocity of the Earth with respect to a reference frame where the halo has no bulk motion.

can be a reasonable one given the fairly narrow energy range probed in the experiments [the signal regions are mainly: 2-4 keVee (DAMA), 0.5-1 keVee (CoGeNT), 12-14 keV (CRESST-II) and 7-13 keV (CDMS/Si)]. With this approximation, the scattering rate depends on the parameters $m_{A'}$, $\epsilon\sqrt{\xi_{A'}}$ and also v_{rot} .

The CDMS/Si experiment has recorded three dark matter candidate events in a 140.2 kg-day exposure of an array of silicon detectors[6]. The nominal recoil energies of these three events are 8.2 keV, 9.5 keV and 12.3 keV. Since the number of events is low we cannot perform a χ^2 analysis. Instead, we use the extended maximum likelihood formalism[23] to construct the likelihood function. This has the form:

$$\mathcal{L}(\mathbf{p}) = \left[\prod_i \frac{dn(E_R^i)}{dE_R} \right] \exp[-\mathcal{N}(\mathbf{p})] \quad (8)$$

where the vector \mathbf{p} denotes the unknown parameters. Here, $dn(E_R^i)/dE_R$ is the expected event rate evaluated at the recoil energy for each of the three observed events, $i = 1, \dots, 3$, and $\mathcal{N}(\mathbf{p})$ is the total number of expected events in the acceptance recoil energy region:

$$\mathcal{N}(\mathbf{p}) = \int \frac{dn}{dE_R} dE_R. \quad (9)$$

The expected event rate, dn/dE_R , is given by the rate dR/dE_R convolved with a Gaussian to take into account the resolution⁵ and multiplied by the detection efficiency, $\epsilon_f(E_R)$ (obtained from figure 1 of ref.[6]).

According to the CDMS paper[6], there are indications that the recoil energy calibration is likely around 10% higher than nominally used, with some uncertainty. We therefore scaled the energies up by a factor, $f = 1.1$ and considered an energy calibration uncertainty of $\pm 10\%$, i.e. $f = 1.1 \pm 0.1$. For each value of $m_{A'}$, $\epsilon\sqrt{\xi_{A'}}$ we have maximized \mathcal{L} over this range of f , to give profile likelihood function, \mathcal{L}_P ⁶. The favoured region for the parameters $m_{A'}$, $\epsilon\sqrt{\xi_{A'}}$ is then determined by the condition

$$\ln \mathcal{L}_P \geq \ln \mathcal{L}_{Pmax} - \Delta \ln \mathcal{L}_P. \quad (10)$$

We fix $2\Delta \ln \mathcal{L}_P = 5.99$ which corresponds to 95% C.L. for 2 parameters[24]. In our scan of parameter space we constrain $m_{A'} \leq m_{Fe'} \simeq 55.8m_p$ (m_p is the proton mass). Note that we neglect backgrounds in this analysis, since the known backgrounds in the energy region of interest, $E_{threshold} \leq E_R \leq 20$ keV, is much less than 1 event.

The analysis of DAMA, CoGeNT and CRESST-II is analogous to our earlier study[7]. As described there, we analyse the DAMA annual modulation signal obtained from the 1.17 ton-year exposure[2]. We consider 12 bins of width 0.5 keVee⁷ from 2 keVee - 8 keVee and evaluate the theoretical annual modulation signal as a function of $m_{A'}$, $\epsilon\sqrt{\xi_{A'}}$, taking into account detector resolution effects. We introduce a χ^2 function in the usual way:

$$\chi^2(m_{A'}, \epsilon\sqrt{\xi_{A'}}) = \sum \left[\frac{R_i - data_i}{\delta data_i} \right]^2. \quad (11)$$

⁵In the absence of resolution measurements, we take $\sigma_{res} = 0.1$ keV.

⁶In our numerical work we let A' , Z' have non-integer values, with $Z' = A'/2$, except when we specifically consider $A' = Fe'$, in which case we use $Z' = 26$, $A' = 55.8$.

⁷The unit keVee is the electron equivalent energy, which is related to nuclear recoil energy via keVee = keV/q, where $q < 1$ is the quenching factor.

v_{rot} [km/s]	CDMS best fit param.	CoGeNT best fit param.	DAMA best fit param.	CRESST-II best fit param.
200	$\frac{m_{A'}}{m_p} = 55.8$ $\frac{\epsilon\sqrt{\xi_{A'}}}{10^{-10}} = 0.93$	$9.7/12$ $\frac{m_{A'}}{m_p} = 39.0$ $\frac{\epsilon\sqrt{\xi_{A'}}}{10^{-10}} = 2.5$	$5.7/10$ $\frac{m_{A'}}{m_p} = 55.8$ $\frac{\epsilon\sqrt{\xi_{A'}}}{10^{-10}} = 2.5$	$2.6/3$ $\frac{m_{A'}}{m_p} = 55.8$ $\frac{\epsilon\sqrt{\xi_{A'}}}{10^{-10}} = 2.7$
240	$\frac{m_{A'}}{m_p} = 37.0$ $\frac{\epsilon\sqrt{\xi_{A'}}}{10^{-10}} = 1.2$	$9.9/12$ $\frac{m_{A'}}{m_p} = 31.0$ $\frac{\epsilon\sqrt{\xi_{A'}}}{10^{-10}} = 3.1$	$5.0/10$ $\frac{m_{A'}}{m_p} = 45.2$ $\frac{\epsilon\sqrt{\xi_{A'}}}{10^{-10}} = 3.6$	$0.3/3$ $\frac{m_{A'}}{m_p} = 55.8$ $\frac{\epsilon\sqrt{\xi_{A'}}}{10^{-10}} = 1.7$
280	$\frac{m_{A'}}{m_p} = 25.5$ $\frac{\epsilon\sqrt{\xi_{A'}}}{10^{-10}} = 1.6$	$10.1/12$ $\frac{m_{A'}}{m_p} = 25.0$ $\frac{\epsilon\sqrt{\xi_{A'}}}{10^{-10}} = 3.6$	$5.2/10$ $\frac{m_{A'}}{m_p} = 37.7$ $\frac{\epsilon\sqrt{\xi_{A'}}}{10^{-10}} = 4.7$	$0.2/3$ $\frac{m_{A'}}{m_p} = 36.0$ $\frac{\epsilon\sqrt{\xi_{A'}}}{10^{-10}} = 2.4$

Table 1: Summary of $\chi^2(\min)$ and best fit parameters for the relevant data sets from the CDMS, CoGeNT, DAMA and CRESST-II experiments.

We then minimize χ^2 over quenching factor uncertainty which we take as: $q_{Na} = 0.28 \pm 0.08$ and $q_I = 0.12 \pm 0.08$. In our analysis we neglect the possibility of channeling[25]⁸. For CoGeNT, we consider the most recent data, stripped of known background components, and corrected for surface event contamination and overall detection efficiency[4]. This data is separated into 15 bins of width 0.1 keVee over the energy range 0.5 - 2 keVee. The resulting χ^2 is minimized over the germanium quenching factor uncertainty which we take as: $q_{Ge} = 0.21 \pm 0.04$ and a constant background contribution. For CRESST-II we bin the data into 5 bins with keV energy ranges of 10.2-13, 13-16, 16-19, 19-25, 25-40. No energy calibration uncertainty is considered for CRESST-II. For each data set, we give 95% C.L. favoured regions [$\chi^2 \leq \chi^2_{\min} + \Delta\chi^2$, with $\Delta\chi^2 = 5.99$]⁹.

In table 1 we summarize the χ^2 minimum values and best fit parameters from each experiment for three representative values of v_{rot} . In figure 1 we plot the favoured region of parameter space for each experiment, for these same v_{rot} values.

⁸There are recent indications that the DAMA quenching factors might be smaller than the considered range[26], and some other indications that the DAMA quenching factors might be larger[27]. Additionally, a few percent channeling fraction for iodine (and also sodium if there are lighter more abundant halo components) can be important which can significantly lower the DAMA favoured region. In view of these uncertainties, the DAMA favoured region should be considered as a rough guide only.

⁹An analysis[28] of the CDMS/Ge low energy data[29] strongly supports [5.7 σ C.L.] a family of low energy events in the nuclear recoil band. Although we don't specifically include the CDMS/Ge data in our analysis here, the study[30] indicates that this data is compatible with the overlapping region of parameter space found in figure 1.

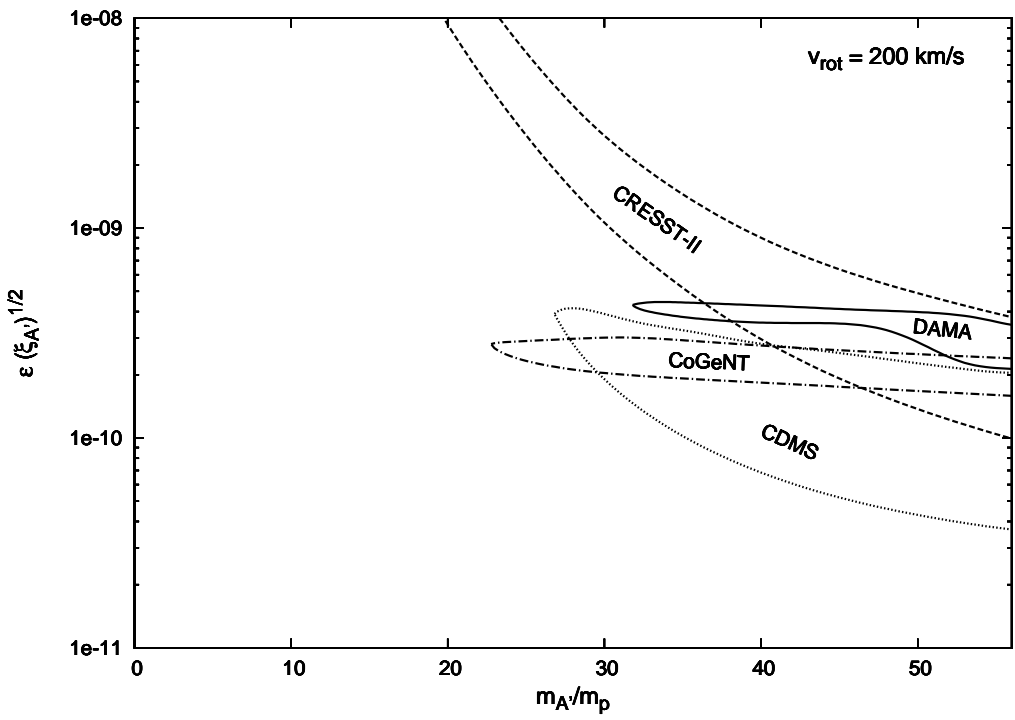


Fig 1a: DAMA (solid lines), CoGeNT (dashed-dotted lines), CRESST-II (dashed lines) and CDMS/Si (dotted lines) favoured regions of parameter space [95% C.L.] in the mirror dark matter model for $v_{rot} = 200$ km/s.

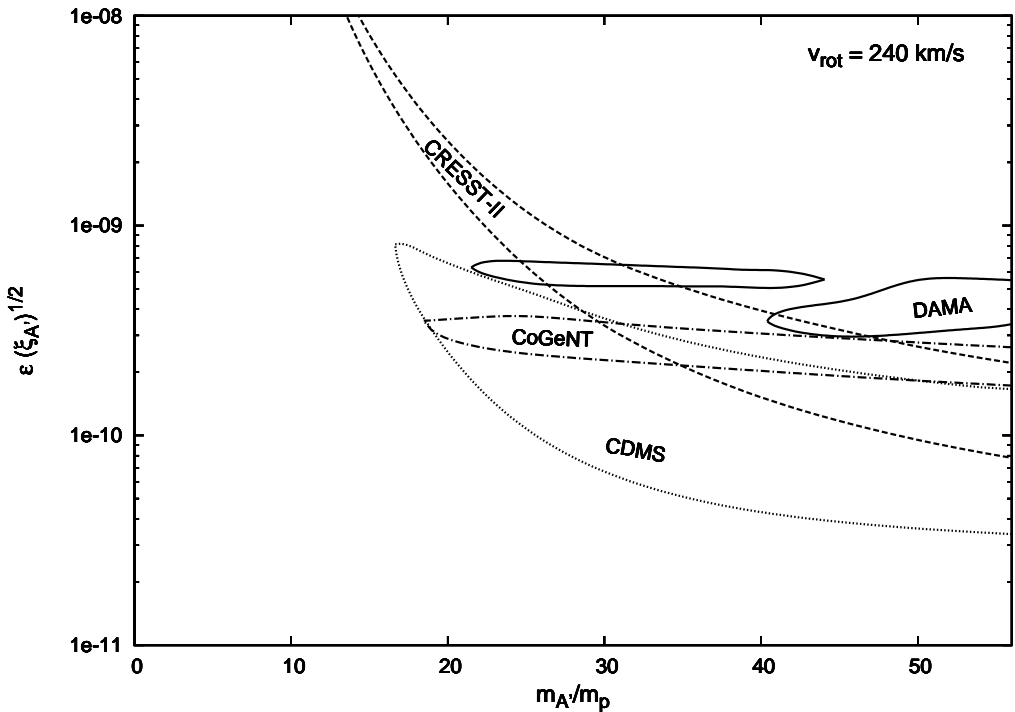


Fig 1b: Same as figure 1a, except $v_{rot} = 240$ km/s.

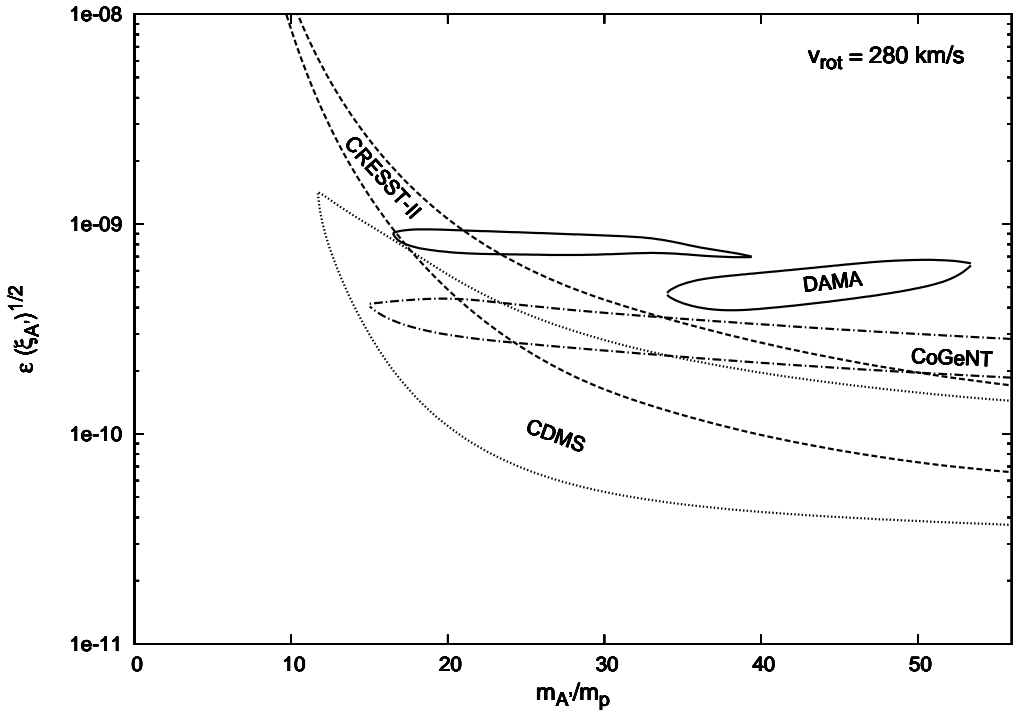


Fig 1c: Same as figure 1a, except $v_{rot} = 280$ km/s.

Figure 1 indicates a substantial region of parameter space where all four experiments can be explained within this theoretical framework. Although this figure suggests that the experiments favour $A' \sim Fe'$, $v_{rot} \approx 200$ km/s, the potential uncertainties cannot exclude other parameter space, with lighter A' components and higher v_{rot} values.

Instead of fixing, v_{rot} and varying $m_{A'} \epsilon \sqrt{\xi_{A'}}$ we also consider fixing A' and treating v_{rot} , $\epsilon \sqrt{\xi_{A'}}$ as free parameters (subject to the mild constraint, $150 \leq v_{rot}[\text{km/s}] \leq 300$). In table 2 we summarize the χ^2 minimum and best fit points for three such fixed A' choices. For each of these choices we have plotted the favoured region of parameter space in figure 2.

$m_{A'}/m_p$	CDMS Z' best fit param.	CoGeNT χ^2 (min)/d.o.f. best fit param.	DAMA χ^2 (min)/d.o.f. best fit param.	CRESST-II χ^2 (min)/d.o.f. best fit param.
55.8		9.3/12	5.5/10	0.3/3
26	$v_{rot} = 205 \text{ km/s}$ $\frac{\epsilon\sqrt{\xi_{A'}}}{10^{-10}} = 0.96$	$v_{rot} = 150 \text{ km/s}$ $\frac{\epsilon\sqrt{\xi_{A'}}}{10^{-10}} = 1.9$	$v_{rot} = 210 \text{ km/s}$ $\frac{\epsilon\sqrt{\xi_{A'}}}{10^{-10}} = 3.1$	$v_{rot} = 250 \text{ km/s}$ $\frac{\epsilon\sqrt{\xi_{A'}}}{10^{-10}} = 1.7$
28.1		9.8/12	9.3/10	0.3/3
14	$v_{rot} = 270 \text{ km/s}$ $\frac{\epsilon\sqrt{\xi_{A'}}}{10^{-10}} = 1.5$	$v_{rot} = 210 \text{ km/s}$ $\frac{\epsilon\sqrt{\xi_{A'}}}{10^{-10}} = 2.5$	$v_{rot} = 280 \text{ km/s}$ $\frac{\epsilon\sqrt{\xi_{A'}}}{10^{-10}} = 8.1$	$v_{rot} = 300 \text{ km/s}$ $\frac{\epsilon\sqrt{\xi_{A'}}}{10^{-10}} = 3.1$
16.0		11.8/12	7.6/10	3.1/3
8	$v_{rot} = 300 \text{ km/s}$ $\frac{\epsilon\sqrt{\xi_{A'}}}{10^{-10}} = 3.5$	$v_{rot} = 300 \text{ km/s}$ $\frac{\epsilon\sqrt{\xi_{A'}}}{10^{-10}} = 3.9$	$v_{rot} = 300 \text{ km/s}$ $\frac{\epsilon\sqrt{\xi_{A'}}}{10^{-10}} = 10.1$	$v_{rot} = 300 \text{ km/s}$ $\frac{\epsilon\sqrt{\xi_{A'}}}{10^{-10}} = 11.0$

Table 2: Summary of $\chi^2(\min)$ and best fit parameters for the relevant data sets from the CDMS, CoGeNT, DAMA and CRESST-II experiments.

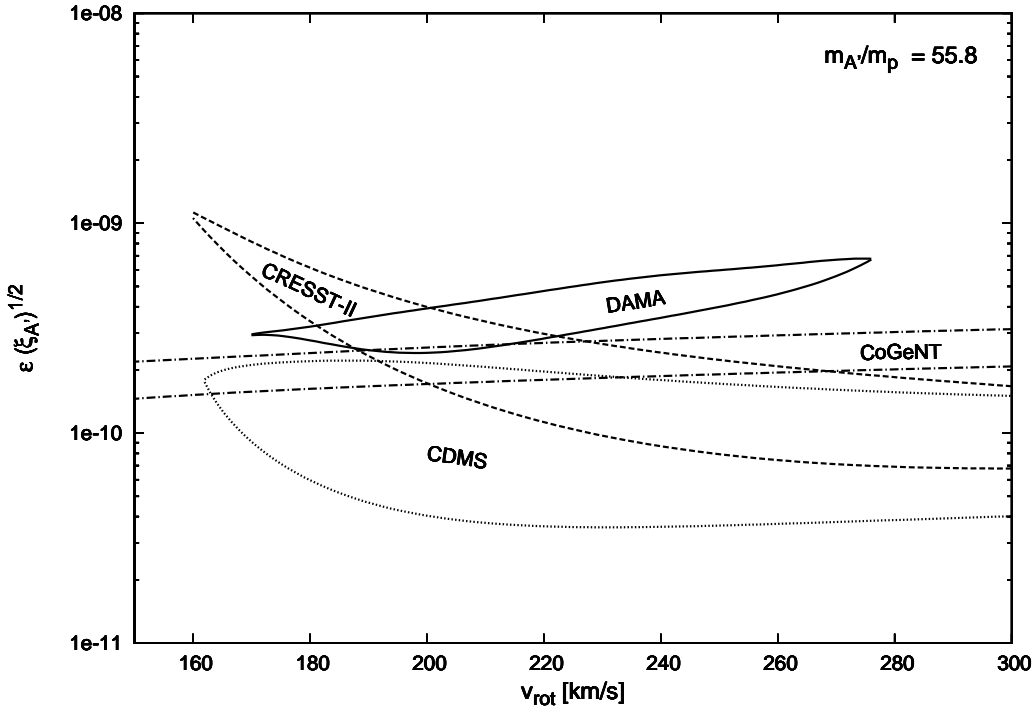


Fig 2a: DAMA (solid lines) , CoGeNT (dashed-dotted lines), CRESST-II (dashed lines) and CDMS/Si (dotted lines) favoured regions of parameter space [95% C.L.] for $A' = Fe'$.

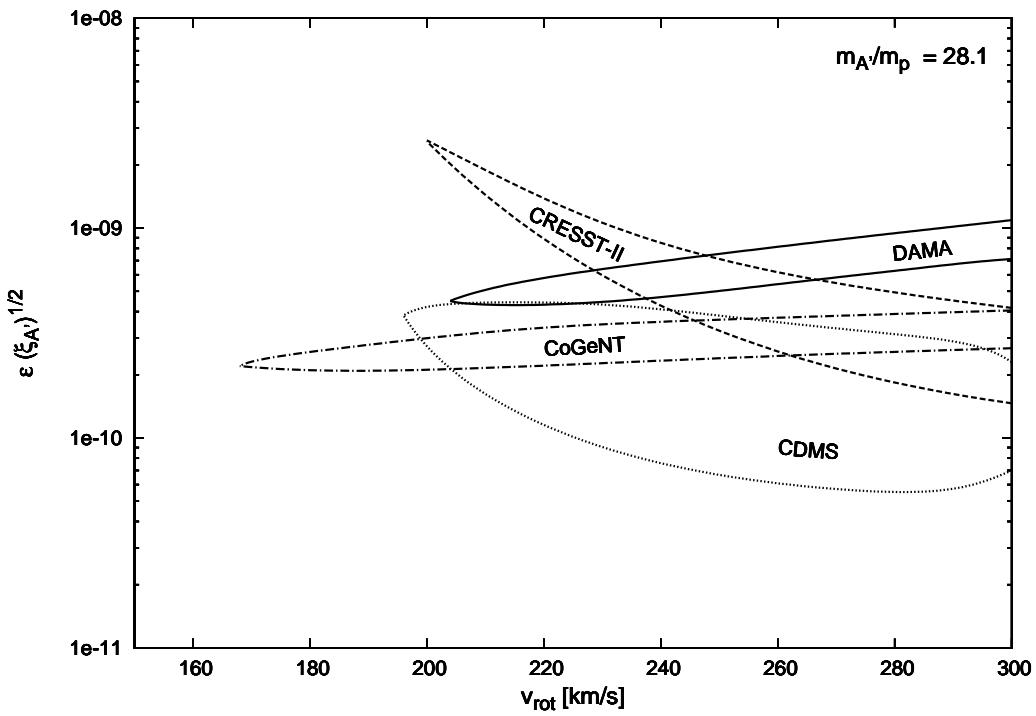


Fig 2b: Same as figure 2a except for $A' = Si'$.

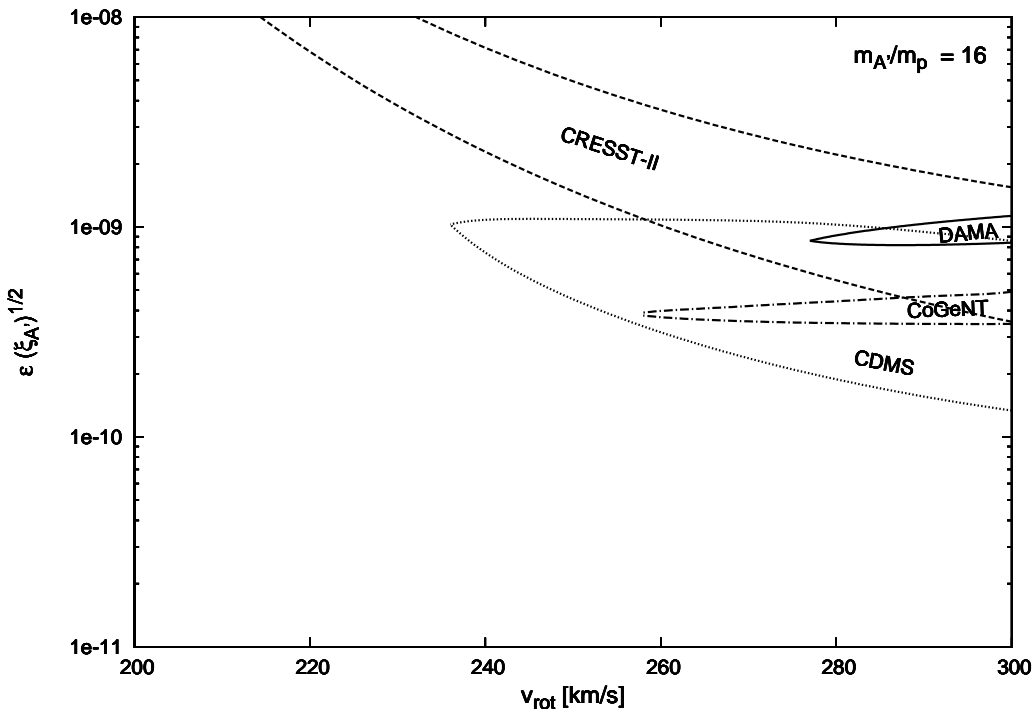


Fig 2c: Same as figure 2a except for $A' = O'$.

If $v_{rot} \sim 200$ km/s and $A' \sim Fe'$ is indeed the component being detected by DAMA, CoGeNT, CRESST-II and CDMS/Si then we expect lower threshold experiments to potentially detect lighter components such as Si' and O' (in addition to Fe'). TEXONO, CDMSlite, C-4, etc might be sensitive to these components. Higher threshold experiments such as XENON100, XENON1T, LUX, XMAS, Edelweiss, etc may only be able to detect the tail of the Fe' halo velocity distribution. This would be manifested as a bunch of events close to threshold. The two events recorded by XENON100[31] and four events by Edelweiss[32] near threshold could be an interesting hint of such an observation.

One might have anticipated XENON100 to have seen a few dozen or so events instead of only 2 events[7]. Thus, the favoured region of parameter space identified in figures 1,2 has significant tension with the current results of the XENON100 experiment[31]. The amount of tension, though, depends sensitively on the systematic uncertainty one assigns for XENON's energy calibration (for recent discussions, see e.g.[33]). For instance the level of tension reduces to zero if the threshold energy is a factor of $\sim 1.5\text{--}2.0$ times higher than the value used by XENON100. Recall the XENON100 experiment has no low energy calibration, but extrapolates the energy scale from measurements of 122 keV X-rays. Importantly, the XENON100 collaboration has plans to check the calibration of their detector in the near future[34] which might help clarify this situation.

Ultimately these very sensitive but higher threshold experiments might also be able to probe the (expected) rare $\sim Pb'$ component. We estimate that the current XENON100 limit on such a component is $\xi_{Pb'}/\xi_{Fe'} \lesssim 10^{-2}$ at 95% C.L. if $\epsilon\sqrt{\xi_{Fe'}} \approx 2 \times 10^{-10}$. On the other hand, if $v_{rot} \sim 240 - 280$ km/s so that $A' \sim Si'$ or O' is being detected by DAMA, CoGeNT, CRESST-II and CDMS/Si then XENON100, XENON1T, LUX, XMAS, Edelweiss etc would be expected to probe the Fe' component. We estimate the current limit on Fe' in this case is $\xi_{Fe'}/\xi_{Si'} \lesssim 10^{-2}$ if $\epsilon\sqrt{\xi_{Si'}} \approx 3 \times 10^{-10}$, $v_{rot} = 240$ km/s and $\xi_{Fe'}/\xi_{O'} \lesssim 10^{-2}$ if $\epsilon\sqrt{\xi_{O'}} \approx 4 \times 10^{-10}$, $v_{rot} = 280$ km/s.

To conclude, the DAMA, CoGeNT, CRESST-II and CDMS/Si results have been examined in the context of the mirror dark matter candidate. In this framework dark matter consists of a spectrum of mirror particles of known masses: e' , H' , He' , O' , Fe' , We find that this theory can simultaneously explain the data from each experiment by $A' \sim Fe'$ interactions if $\epsilon\sqrt{\xi_{Fe'}} \approx 2 \times 10^{-10}$ and $v_{rot} \sim 200$ km/s. Other parameter regions, and also, more generic hidden sector dark matter models are also possible. Further direct tests of this dark matter framework are expected in the near future from higher precision experiments such as C-4, CDEX, superCDMS, COUPP, LUX, PandaX etc. These and other experiments should provide further scrutiny of mirror dark matter and closely related hidden sector models in the near future.

Acknowledgments

This work was supported by the Australian Research Council.

References

- [1] R. Bernabei *et al.* (DAMA Collaboration), Riv. Nuovo Cimento. **26**, 1 (2003); Int. J. Mod. Phys. E**13**, 2127 (2004); Phys. Lett. B**480**, 23 (2000).

- [2] R. Bernabei *et al.* (DAMA Collaboration), Eur. Phys. J. C**67**, 39 (2010); Eur. Phys. J. C**56**, 333 (2008).
- [3] C. E. Aalseth *et al.* [CoGeNT Collaboration], Phys. Rev. Lett. **106**, 131301 (2011); Phys. Rev. Lett. **107**, 141301 (2011).
- [4] C. E. Aalseth *et al.* [CoGeNT Collaboration], arXiv:1208.5737.
- [5] G. Angloher *et al.*, Eur. Phys. J. C **72**, 1971 (2012).
- [6] R. Agnese *et al.* [CDMS Collaboration], arXiv:1304.4279.
- [7] R. Foot, Phys. Rev. D **86**, 023524 (2012).
- [8] R. Foot, arXiv:1211.1500.
- [9] R. Foot, Phys. Rev. D**69**, 036001 (2004); Mod. Phys. Lett. A**19**, 1841 (2004); Phys. Rev. D**78**, 043529 (2008); Phys. Rev. D**81**, 087302 (2010); Phys. Rev. D**82**, 095001 (2010); Phys. Lett. B**692**, 65 (2010); Phys. Lett. B **703**, 7 (2011); JCAP **1204**, 014 (2012).
- [10] Z. K. Silagadze, Acta Phys. Polon. B **32**, 99 (2001); A. Y. Ignatiev and R. R. Volkas, hep-ph/0306120; R. Foot, Int. J. Mod. Phys. D**13**, 2161 (2004); Int. J. Mod. Phys. A**19** 3807 (2004); Z. Berezhiani, Int. J. Mod. Phys. A **19**, 3775 (2004). P. Ciarcelluti, Int. J. Mod. Phys. D**19**, 2151 (2010).
- [11] J. -W. Cui, H. -J. He, L. -C. Lu and F. -R. Yin, Phys. Rev. D **85**, 096003 (2012); R. Foot, arXiv:1209.5602; Phys. Lett. B **703**, 7 (2011).
- [12] R. Foot, H. Lew and R. R. Volkas, Phys. Lett. B**272**, 67 (1991); Mod. Phys. Lett. A**7**, 2567 (1992); R. Foot and R. R. Volkas, Phys. Rev. D **52**, 6595 (1995).
- [13] R. Foot and X-G. He, Phys. Lett. B**267**, 509 (1991).
- [14] B. Holdom, Phys. Lett. B **166**, 196 (1986).
- [15] R. H. Helm, Phys. Rev. **104**, 1466 (1956).
- [16] J. D. Lewin and P. F. Smith, Astropart. Phys. **6**, 87 (1996).
- [17] R. Foot and R. R. Volkas, Phys. Rev. D**70**, 123508 (2004).
- [18] R. Foot and Z. K. Silagadze, Int. J. Mod. Phys. D **14**, 143 (2005).
- [19] P. Ciarcelluti and R. Foot, Phys. Lett. B **679**, 278 (2009); R. Foot, Phys. Lett. B **711**, 238 (2012); Phys. Lett. B **718**, 745 (2013).
- [20] P. Ciarcelluti and R. Foot, Phys. Lett. B**690**, 462 (2010).
- [21] R. Foot, Phys. Lett. B **699**, 230 (2011).
- [22] R. Foot, Phys. Rev. D **88**, 023520 (2013).

- [23] R. Barlow, Nucl. Instrum. Methods A **297**, 496 (1990).
- [24] J. Beringer *et al.* [Particle Data Group Collaboration], Phys. Rev. D **86**, 010001 (2012).
- [25] N. Bozorgnia, G. B. Gelmini and P. Gondolo, JCAP **1011**, 019 (2010).
- [26] J. I. Collar, arXiv:1302.0796; arXiv:1303.2686.
- [27] V. I. Tretyak, Astropart. Phys. **33**, 40 (2010).
- [28] J. I. Collar and N. E. Fields, arXiv:1204.3559.
- [29] Z. Ahmed *et al.* [CDMS-II Collaboration], Phys. Rev. Lett. **106**, 131302 (2011); arXiv:1203.1309.
- [30] R. Foot, arXiv:1211.3217.
- [31] E. Aprile *et al.* [XENON100 Collaboration], Phys. Rev. Lett. **109**, 181301 (2012).
- [32] E. Armengaud *et al.* [EDELWEISS Collaboration], Phys. Lett. B **702**, 329 (2011).
- [33] J. I. Collar, arXiv:1106.0653; arXiv:1010.5187.
- [34] A. Melgarejo, on behalf of the XENON100 collaboration, talk at *light dark matter* workshop, April 2013.